PROCEEDINGS OF SCIENCE

Extensive Air Shower (EAS) Development in the Upper Atmosphere: a unique environment to measure the EAS properties

John F. Krizmanic,[a,*] **Austin L. Cummings,**[b] **Fred A.B. Garcia**[c] **and John W. Mitchell**[a]

[a] *NASA/GSFC*
Laboratory for Astroparticle Physics
8800 Grenbelt Rd, Greenbelt, Maryland 20771, USA
[b] *Departments of Physics and Astronomy Astrophysics*
Institute for Gravitation and the Cosmos
Pennsylvania State University
University Park, PA 16802, USA
[c] *Deptment of Physics*
University of Maryland
Colledge Park, Maryland 20742, USA

E-mail: john.f.krizmanic@nasa.gov

The direct observation of the beamed, radio and optical Cherenkov signals from cosmic-ray induced extensive air showers (EAS) viewed above-the-Earth-limb offers a unique environment to study the EAS development in the rarified atmosphere. ANITA has measured the beamed, geomagnetic radio signal from EAS from UHECRs, and initial analysis of measurements by EUSO-SPB2 are consistent with the beamed, optical Cherenkov signal from cosmic rays above approximately 1 PeV. For an observation at 33 km altitude, the horizontal slant depth of the atmosphere corresponds to $\sim$ 300 g/cm^2 while the slant depth quickly increases when viewing closer to the limb. Thus, an instrument can be within the early part of the EAS development while the distance and the atmospheric absorption depth will be small for X-rays generated by high-energy electron synchrotron radiation. The rarified atmospheric environment where these EAS develop is such that the nuclear interaction length is much larger in distance that the Coulomb scattering length, providing a probe of hadronic interactions. Furthermore, the optical attenuation in for Cherenkov light is minimal for these near horizontal EAS, implying that this signal from both the EM bulk of the EAS and that from the muon tail can be both observed as well as the muons themselves. In this paper, we evaluate these disparate EAS signals, radio, optical, HE photon, and particle distributions, and outline the use of these as a tool to measure the cosmic ray and EAS properties in a shower development regime inaccessible to accelerator-based experiments.

38th International Cosmic Ray Conference (ICRC2023)
26 July - 3 August, 2023
Nagoya, Japan

*Speaker

PoS(ICRC2023)524

1. Properties of Upward-Moving Extensive Air Showers (EAS)

One of the unique features of predicting the optical Cherenkov [1–3] and geomagnetic radio [4] signals from upward-moving extensive air showers (EAS) from τ-lepton decay induced by tau neutrinos in the Earth is the understanding of the EAS development in the rarified atmosphere. Key aspects of this effect is shown in Figs. 1 and 2. The Fig. 1 shows the fraction of τ-leptons that decay above an altitude of 16 km, which is the altitude where the atmospheric pressure is approximately a tenth of that at sea level. The τ-lepton decay fraction is shown as function of τ-lepton Earth-emergence angle, which is aligned to the incident tau neutrino trajectory through the Earth, and the τ-lepton energy. The results show that at higher Earth-emergence angles and energies, a significant fraction of the EAS formed from τ-lepton decay will occur in the rarified atmosphere. The impact of this is shown in Fig. 2, which shows the longitudinal EAS profile as a function of pion-induced EAS starting point for τ-leptons with $\beta_E = 5°$. For starting altitudes around 15 km and higher, the EAS development and evolution becomes inhibited by the lack of target material in the atmosphere to continue the EAS development. Another effect that also becomes important in the rarified is the spread due to geomagnetic effects [5, 6]. The angular spread of the charged particles in an EAS, usually dominated by electrons and positrons, strongly effect the strength and spatial distribution of the observed optical Cherenkov and radio emission. The angular spread is due to Coulomb scattering and if the spatial length for a given slant depth, in g/cm^2, becomes long, geomagnetic effects can become a dominant effect.

The relationship between interaction lengths and decay lengths is modified in a rarified atmosphere. Fig. 3 shows this effect in the comparison of five EAS profiles for CONEX [8] generated proton EAS where the 100 TeV protons are injected at 10 km altitude with a trajectory defined by $\beta_E = 5°$. The nature of the rarified atmosphere leads to relatively long spatial scales between interactions leading

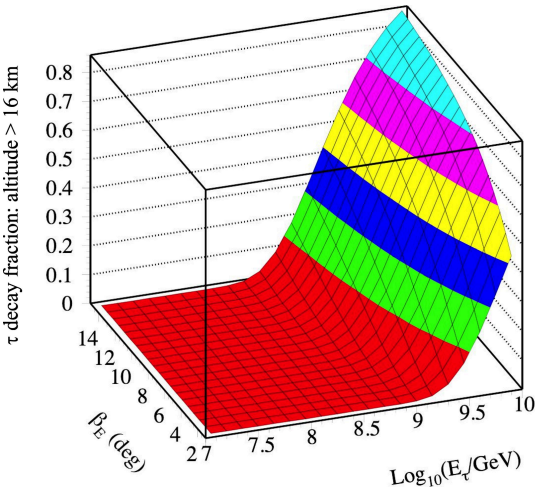

Figure 1: The fraction of τ-leptons that decay at an altitude larger than 16 km as a function of Earth-emergence angle (β_E) and $\log_{10}(E_\tau/\text{GeV})$. The colored bands show 0.1 increments of the τ-lepton decay fraction.

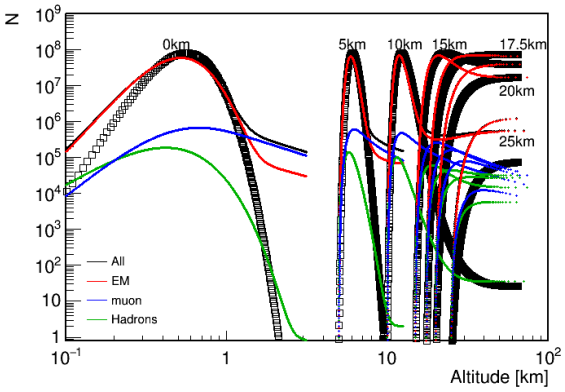

Figure 2: The average longitudinal EAS profiles from the CONEX simulation for 100 PeV pions (1000 events) for 5° Earth-emergence angle as a function of EAS starting altitudes. The various components are shown by the solid lines while the black boxes show the profile based from the Greisen parameterization for 100 PeV.

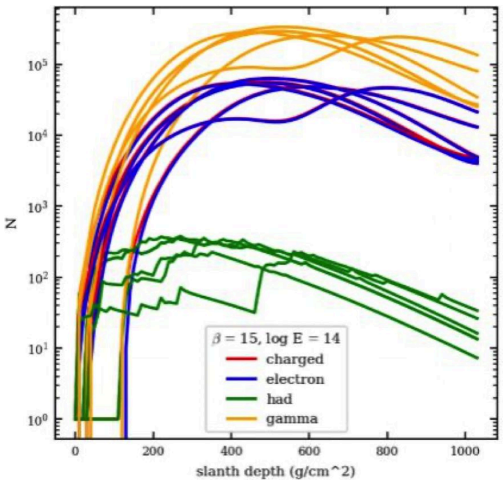

Figure 3: The CONEX-generated longitudinal profiles of five different 100 TeV proton-induced EAS started at 10 km altitude. The trajectory geometry is aligned with a 5° Earth-emergence angle (or 85° zenith angle) at sea level.

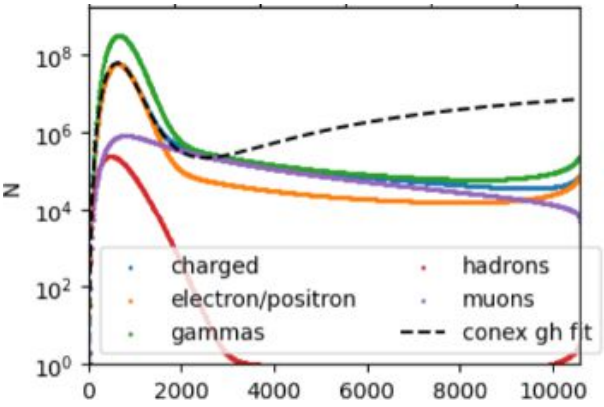

Figure 4: The EAS profiles of the various components of an EAS from the CONEX simulation for 100 PeV protons for $\beta_E = 5°$ Earth-emergence angle starting at sea level. The tails are dominated by muons but with a $\sim 10\%$ $e^{\pm}$ from muon decay. The Gaisser-Hillas [7] is provided by CONEX showing the fit is tuned to fit the bulk of the shower: the quadratic fit in the λ parameter causes the fit to diverge for deeper slant depths.

to individual interactions producing distinctive structure in the electromagnetic component of the EAS. Additionally, the slant depth of the EAS before all muons decay can be very long, and this is shown in Fig. 4. As opposed to downward-moving EAS where the surface of the Earth provides a 'beam stop', there is nothing to stop the development of upward-moving EAS. The development in both slant depth and spatial length can be quite long as shown in Fig. 4, especially due to the muon tail that feed a smaller electron/positron component via muon decay.

2. Properties of Nearly-Horizontal, Upward-Moving Cosmic Ray EAS

Cosmic rays that interact in the atmosphere that have trajectories in the direction of a balloon-borne or space-based instrument can also provide significant EAS optical Cherenkov emission [9] and geomagnetic radio emmission [10, 11]. These cosmic ray events are viewed from the direction a few degrees above the Earth's limb for instruments at balloon altitudes or low-Earth orbit. Fig. 5 illustrates the cosmic-ray trajectory in relation to Cherenkov emission and detection by an instrument at a high altitude. Setting the altitude to 33 km, that of balloon-borne instruments, the Earth limb is $\sim 84.2°$ away from the nadir direction. The slant depth as a function of angle away from nadir and greater than 84.2° is shown in Fig. 6 assuming an altitude of 33 km. The curve demonstrates that the viewed depth of the atmosphere becomes less that 10^3 g/cm^2 for viewing angles $\sim 4°$ above the limb (or $\sim 88°$ from nadir. For angles approaching 90° from nadir, or trajectories viewed horizontal from 33 km, the depth becomes $\lesssim 500$ g/cm^2.

A comparison of Figs. 4 and 6 presents an interesting physical configuration for viewing angles near 90° from nadir for an instrument at 33 km: the instrument can be located within the bulk of the EAS development. Additionally, for deeper slant depths the muon tail may provide a distinctive

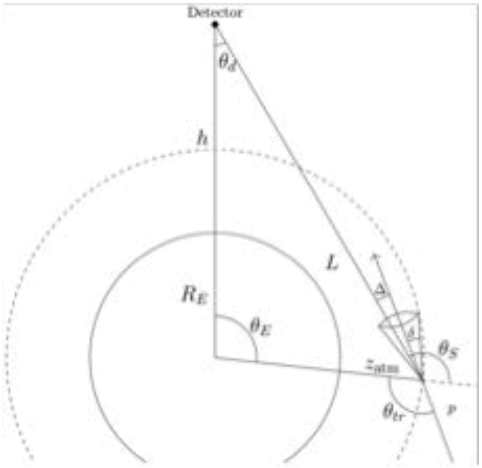

Figure 5: The geometry for a the optical Cherenkov signal from cosmic-ray EAS viewed above the Earth's limb. From Ref. 9, DOI:10.1103/PhysRevD.104.063029

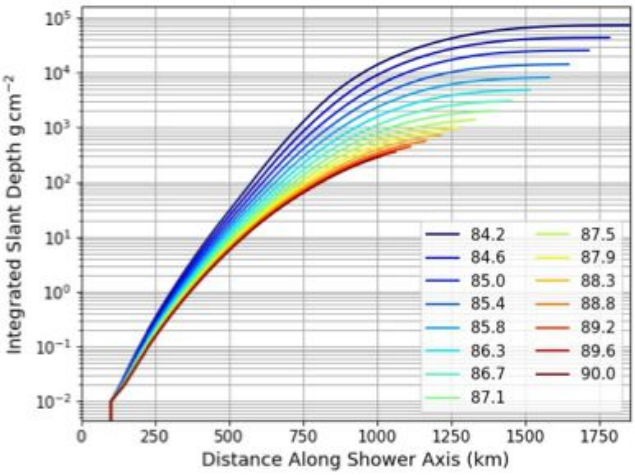

Figure 6: The slant depth through the atmosphere as a function of distance to the EAS starting poing for various angles from nadir, viewed from an altitude of 33 km. The Earth's limb is located at 84.2° from nadir.

Cherenkov signal [12, 13]. In terms of cosmic ray rates, these have been calculated for the EUSO-SPB2 [14] ULDB payload's Cherenkov Camera and the results are presented in Fig. 7. The results show that for a EUSO-SPB2 size Chernekov telescope , with a field-of-view of $6.4° \times 12.6°$ and 0.7 m^2 effective optical collecting area, will have a threshold around 1 PeV, has a predicted rate of $\sim$ 200 observed cosmic rays per live-time hour when the CT is tilted above the Earth's limb. The rate is only a factor of 10 lower for a 10 PeV threshold due to the growth of the geometry factor as the energy increases before it starts to saturate. These results include taking into account the optical attenuation of the Cherenkov light from aerosols, Rayleigh scattering, and ozone. In fact, the atmosphere acts as an cosmic ray energy filter for these events viewed above the Earth's limb as shown in Fig. 8. The rate is correlated to the inverse of the slant depth due to the different energy thresholds for accepting cosmic ray events.

Estimate of EAS Particle Densities at Balloon Altitudes: As indicated in the comparisons Fig. 4 and 6, there are cosmic ray trajectories that can lead to a balloon-borne instrument being within the EAS particle distribution. The focal plane of the EUSO-SPB2 is $\sim$ 200 cm^2 in area, and the EAS particle flux may be detectable. However, since these EAS are developing in the rarified atmosphere the particle fluxes are low. The electromagnetic component of an EAS has a characteristic lateral width given by the Molière radius, which is 8.33 g/cm^2 in air. Fig. 9 presents the cumulative distribution functions (CDFs) as a function of shower age using the NKG [15, 16] parameterization of the transverse width: $\rho(r) \propto (r/r_M)^{s-2}(1 + (r/r_M))^{s-4.5}$, where r_M is the Molière radius and s is the shower age. The curves show that the lateral width of the EAS electron distribution is slightly more that a Molière radius around shower maximum ($s = 1$ and then grows larger as function of shower age. Converting the Molière radius to a distance scale at different altitudes, as shown in Fig. 10, the Molière radius has a length scale of kilometers at altitudes at and above 20 km. Fig. 11 presents the altitude of closest approach for a trajectory defined by the

angular range for observation from 33 km of above-the-limb cosmic-ray trajectories. Comparing this to the results shown in Figs. 6 and 8 for the condition where the slant depth is $\lesssim 10^3$ g/cm^2, this indicates that the Molière radius is much larger than a kilometer. Thus the particle densities in an EAS even at shower maximum will be small, e.g. at 10^7 GeV, the charged particle density in $< 10^{-3}$ particles/cm^2. This implies that the detection of the particles themselves will require square-meter of larger detector area.

This also implies that some of the EAS optical Cherenkov light will be generated from far from the cosmic ray trajectory axis. Geomagnetic effects on the electrons and positrons trajectories further affects the nature of the EAS Cherenkov light emission at high altitudes. These near-field effects will lead to a distinctive pattern on a Cherenkov telescope's focal plane providing a signature of the EAS when near the instrument. This combined with the Cherenkov timing information can a further measure of the cosmic ray trajectory. As shown in Fig. 12, the Cherenkov time spread profile as a function of viewing angle away from cosmic ray trajectory provides a determination whether the observation is within the Cherenkov cone, where the temporal spread is of the order of 10 ns, or outside the cone where the temporal spread is a function of direction of the cosmic ray trajectory away from the viewing angle.

X-ray Signal from e$^{\pm}$ Synchrotron and Bremsstrahlung Radiation: Electrons and positrons with energies in the TeV range will create synchrotron radiation in the X-ray band [20]. Given that the EAS are developing in a rarified atmosphere and potentially close to a balloon-borne instrument, the X-ray signal from TeV e$^{\pm}$ in the EAS may be observable. Fig. 13 shows the prediction of the electron energy distribution as a function of shower age up to 10 TeV. The results demonstrate that early in the EAS development, the trans-TeV electron population is significant. This in turn will providing a strong X-ray signal which is shown in Fig. 14. Fig. 15 presents the attenuation length in air as a function of photon energy. Evaluated at an altitude of 30 km, the attenuation length at 30 keV corresponds to $\sim$ 2 km and the attenuation length at 1 MeV is $\sim$ 12 km. This implies the

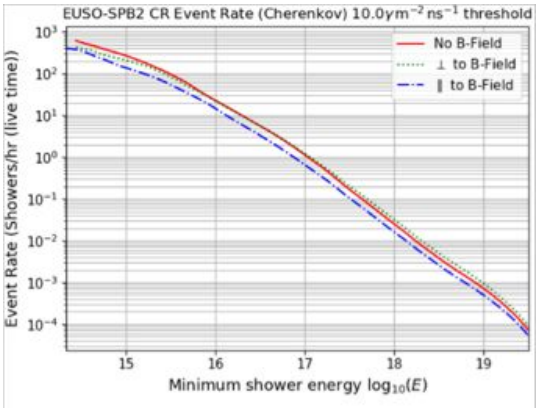

Figure 7: Predicted integrated event rates for above-the-limb cosmic ray events using the EUSO-SPB2 Cherenkov telescope. From Ref. 9, DOI:10.1103/PhysRevD.104.063029

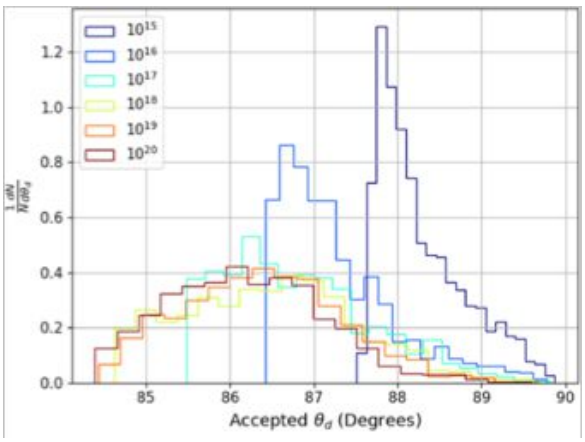

Figure 8: The normalized arrival angle distributions for cosmic rays simulated for the EUSO-SPB2 experiment for different primary proton energies. From Ref. 9, DOI:10.1103/PhysRevD.104.063029

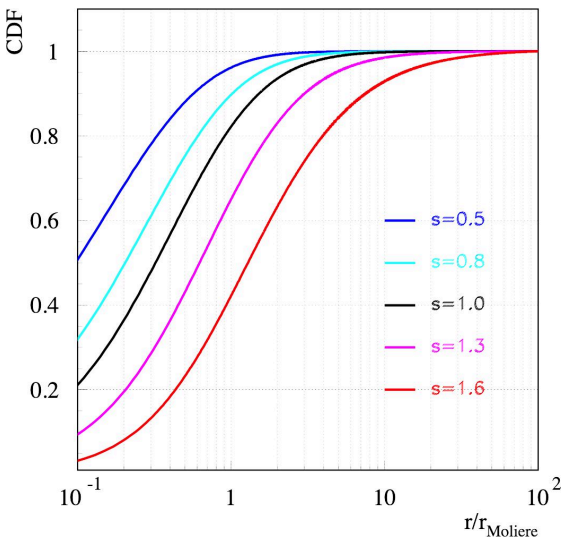

Figure 9: The prediction of EAS electron transverse width in terms of Molière radius as a function of shower age.

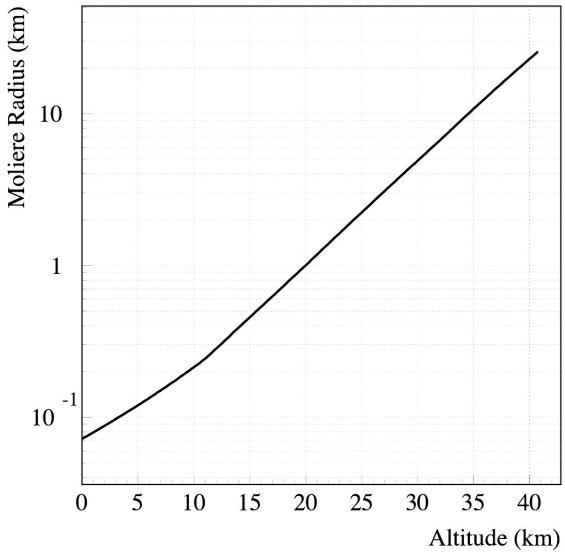

Figure 10: The Molière radius in the atmosphere as a function of altitude assuming $R_{Moliere} = 8.83 g/cm^2$ and the 1976 Standard atmosphere.

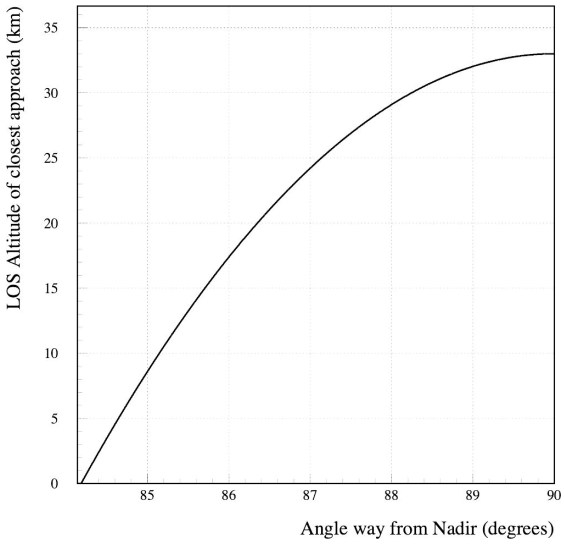

Figure 11: The altitude at closest approach to the Earth surface for the line-of-sight vector from 33 km and as a function of angle away from nadir.

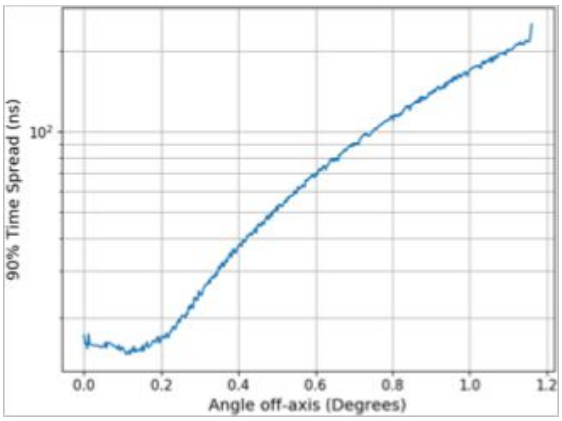

Figure 12: The 90% contained time width of the optical Cherenkov signal as a function of angle away from the EAS trajectory. The observation is at an altitude of 33 km and the 100 PeV proton EAS was generated at a viewing angle 85° from nadir. From Ref. 9, DOI:10.1103/PhysRevD.104.063029

X-ray spectrum from trans-TeV electrons in the EAS can be measured, implying the high-energy population at early shower age can be measured. Furthermore, the strong absorption below 30 keV could provide a diagnostic to whether an EAS is close to a balloon-borne detector or not. While to fully understand this potential, full 3-dim modeling of the EAS electrons in the rarified atmosphere is required, this initial analysis is very encouraging. That is there appears to be a way to measure the $e^{\pm}$ energy distributions as a function of EAS age while via measuring the X-ray spectrum that

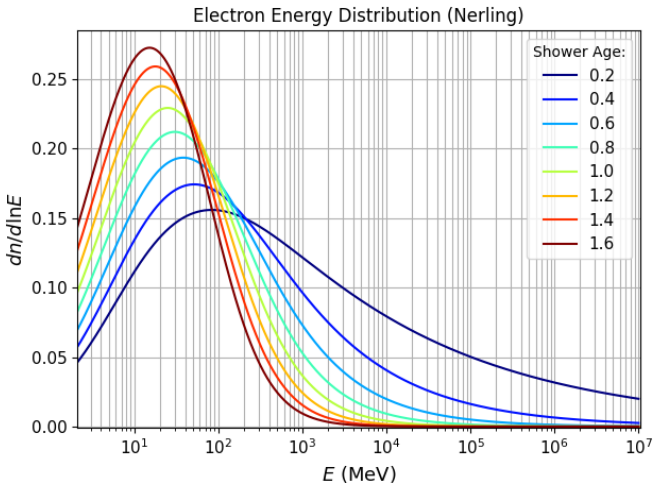

Figure 13: The EAS electron energy distribution as a function of shower age as defined in 17.

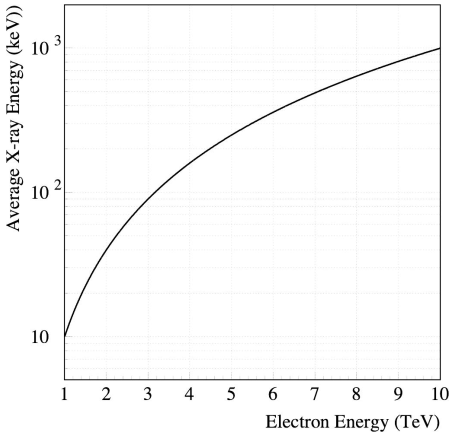

Figure 14: The average synchrotron X-ray energy as a function of the emitting electron energy in the geomagnetic field (B=50 μT).

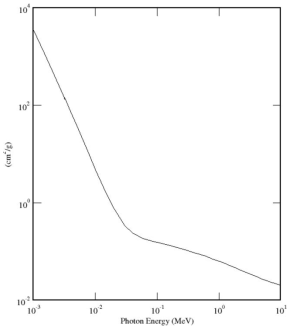

Figure 15: The air attenuation factor for photons from 1 keV to 10 MeV as reported by a NIST XCOM [18] calculation.

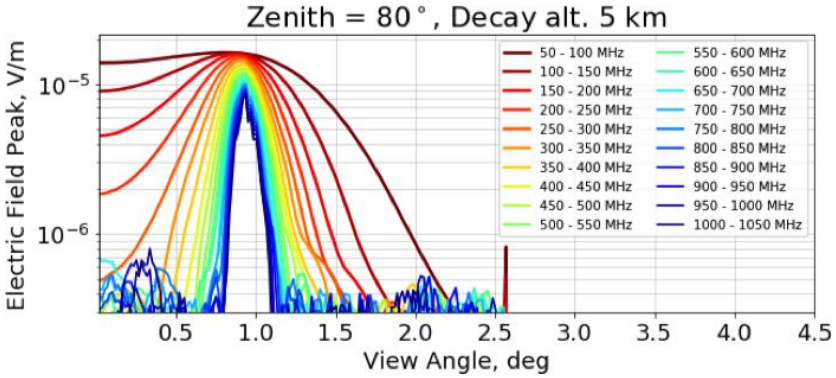

Figure 16: The EAS radio signal as a function of angle from the trajectory and emission frequency for a simulated upward-moving EAS that began at 8 km with an 80° zenith angle. From Ref. 19.

would be observed at balloon-borne instrument.

3. Discussion

The results from the EUSO-SPB2 flight confirms predictions that the cosmic ray observation rates are consistent with ~ 200/live-timeHour for $E_{\rm CR} \geq 1$ PeV, indicating a large sample, ~ 100,000 events in 500 live hours (100-day balloon flight) could be achievable. Given the potential for a high-statistics cosmic-ray measurement from below and through the knee (~ $10^{6.5}$ GeV) could be achievable. In this paper, several of the unique aspects of EAS development in the rarified, upper atmosphere are discussed to understand if EAS measurements in the rarified atmosphere could be used to measure the hadronic and EM EAS processes including muon production since a significant fraction of events will be measured within the EAS development and at early ages. We have performed a initial analysis the context of over-the-limb cosmic ray EAS optical Cherenkov, and potentially X-ray signals. The addition of EAS geomagnetic radio measurements could provide a constraint to provide a determination of the distance to shower maximum, which translates in an

$X_{\rm max}$measurement. Fig. 16 presents the peak external electric field measured at an high altitudes for a 100 PeV proton EAS that started at 8 km altitude. The frequency response of the radio profile provides a measure of the Cherenkov angle for those events seen near the Cherenkov ring. Since the Cherenkov angle is a function of altitude, this measurement would determine the altitude at shower maximum. This determines the geometry of the trajectory and location of $X_{\rm max}$, potentially providing a method to measure the cosmic ray nuclear composition. These results motivate the need for further study to determine the full potential of measuring above-the-limb cosmic rays using ULDB balloon-borne instruments.

4. Acknowledgements

This work is supported by NASA RTOP 21-APRA21-0071 and NASA RTOP 21-APRA21-0009 at GSFC and NASA grant 80NSSC22K1519 at PennState.

References

[1] M. H. Reno, J. F. Krizmanic, and T. M. Venters, Phys. Rev. D **100**, 063010 (2019).

[2] T. M. Venters, M. H. Reno, J. F. Krizmanic, L. A. Anchordoqui, C. Guépin, and A. V. Olinto, Phys. Rev. D **102**, 123013 (2020).

[3] A. L. Cummings, R. Aloisio, and J. F. Krizmanic, Phys. Rev. D **103**, 043017 (2021), 2011.09869.

[4] P. W. Gorham, B. Rotter, P. Allison, O. Banerjee, L. Batten, J. J. Beatty, K. Bechtol, K. Belov, D. Z. Besson, W. R. Binns, et al., Phys. Rev. Lett. **121**, 161102 (2018).

[5] G. Cocconi, Phys. Rev. **93**, 646 (1954).

[6] G. Cocconi, Phys. Rev. **95**, 1705 (1954).

[7] T. K. Gaisser and A. M. Hillas, in *Proceedings of the 15th ICRC (Plovdiv)* (1977), vol. 8, pp. 353–357.

[8] T. Pierog, M. K. Alekseeva, T. Bergmann, V. Chernatkin, R. Engel, D. Heck, N. N. Kalmykov, J. Moyon, S. Ostapchenko, T. Thouw, et al., Nuclear Physics B Proceedings Supplements **151**, 159 (2006), astro-ph/0411260.

[9] A. L. Cummings, R. Aloisio, J. Eser, and J. F. Krizmanic, "Phys. Rev. D", **104**, 063029 (2021), 2105.03255.

[10] S. Hoover, J. Nam, P. W. Gorham, E. Grashorn, P. Allison, S. W. Barwick, J. J. Beatty, K. Belov, D. Z. Besson, W. R. Binns, et al., Phys. Rev. Lett. **105**, 151101 (2010), 1005.0035.

[11] P. W. Gorham, A. Ludwig, C. Deaconu, P. Cao, P. Allison, O. Banerjee, L. Batten, D. Bhattacharya, J. J. Beatty, K. Belov, et al., Phys. Rev. Lett. **126**, 071103 (2021).

[12] A. Neronov, D. V. Semikoz, I. Vovk, and R. Mirzoyan, Phys. Rev. D **94**, 123018 (2016), 1610.01794.

[13] D. Fuehne, T. Heibges, et al., in *Proceedings of the 38th ICRC* (2023), PoS(ICRC2023)363.

[14] J. Eser, L. Olinto, Angela V. Wiencke, et al., in *Proceedings of the 38th ICRC* (2023), PoS(ICRC2023)397.

[15] G. Puppi, H. Bridge, and K. Greisen, *Progress in Cosmic Ray Physics. Vol. 3. Edited by J.G. Wilson ... Contributors: K. Greisen, H.S. Bridge, R.W. Thompson, G. Puppi* (North-Holland Publishing C°, 1956), URL https://books.google.com/books?id=V_E8ygAACAAJ.

[16] K. Kamata and J. Nishimura, Progress of Theoretical Physics Supplement **6**, 93 (1958).

[17] F. Nerling et al., Astropart. Phys. **24**, 421 (2006).

[18] See https://physics.nist.gov/PhysRefData/Xcom/html/xcom1.html.

[19] J. Krizmanic, PoS **ICRC2021**, 1205 (2021).

[20] A. M. Galper, S. V. Koldashov, V. V. Mikhailov, and O. F. Prilutskii, in *Journal of Physics Conference Series* (2017), vol. 798 of *Journal of Physics Conference Series*, p. 012176.